Statistical Analysis of Urban GPS Multipaths and Pseudo-Range Measurement Errors

SEUNG-HYUN KONG, Member, IEEE
Korea Advanced Institute of Science and Technology

In urban environments one of the causes of pseudo-range measurement error in Global Positioning System (GPS) is short-delay multipaths due to the scatterers around the receiver. Therefore knowledge of the temporal distribution of GPS multipaths based on a statistical scatterer distribution in an urban environment is essential to estimating the positioning performance and to developing an efficient multipath mitigation technique for urban GPS applications. The work presented here introduces a scatterer distribution model for the urban environment, derives analytical expressions of the consequent time-of-arrival (TOA) probability density function (pdf) with respect to satellite elevation angles, and analyzes the effect of short-delay multipaths on the pseudo-range measurement errors. The expressions derived provide insights into the statistical properties of GPS multipaths and pseudo-range measurement errors in GPS code phase measurement functions due to the short-delay multipaths.

Manuscript received September 7, 2008; revised March 20, August 10, and October 16, 2009; released for publication December 10, 2009.

IEEE Log No. T-AES/47/2/940832.

Refereeing of this contribution was handled by G. Lachapelle.

Author's address: Department of Aerospace Engineering, Korea Advanced Institute of Science and Technology (KAIST), Daejeon, Republic of Korea.

I. INTRODUCTION

Statistical distribution of time-of-arrival (TOA) of Global Positioning System (GPS) multipaths depends on physical scatterer distribution around a GPS receiver. In dense urban areas the heights and density of buildings or objects around the GPS receiver are much higher than in rural areas, so the probability of receiving a line-of-sight (LOS) path is very low, and large multipath delays are not uncommon [1]. In [2] and [3], precise measurements of statistical distributions of scatterers and multipath delays of simulated wideband satellite signal transmitted from a Zeppelin at a high altitude in urban environments are introduced. In [2], it is shown that the TOA probability density of a satellite signal is decreasing with multipath delay and that the TOA pdf becomes narrower as the elevation angle increases. In [3], likelihood distribution of scatterers with respect to the relative azimuth angle between the simulated satellite and scatterer is introduced. Despite many field observations to understand the properties of GPS multipaths in urban environments, there have been few studies to mathematically explain the elevation-angle-dependent statistical distribution of GPS multipath delays from a generalized scatterer distribution.

The knowledge of TOA pdf of GPS multipaths provides substantial insights into the distribution of the non-line-of-sight (NLOS) delay errors and into the distribution of pseudo-range measurement errors. Multipaths cause various errors in GPS, and one of the most unpredictable and difficult errors to mitigate in the GPS receiver is the pseudo-range measurement error due to short-delay multipaths. The effect of short-delay multipaths on pseudo-range measurement function has been analyzed by [4], [5], and [6], assuming that the first arrival path is stronger than other later arrival multipaths. In many urban indoor and outdoor environments, however, the first arrival path may not be the strongest path when the LOS path is blocked or severely attenuated due to buildings or obstacles around the receiver.

The urban environment is one of the most challenging environments for GPS, and this paper presents mathematical analysis of statistical distribution of scatterers that varies with satellite elevation, consequent TOA pdf of GPS multipaths, and pseudo-range measurement errors due to the short-delay multipaths. Section II discusses modeling the statistical distribution of scatterers around a GPS receiver in urban environments, and Section III derives consequent mathematical expression of the TOA pdf. It is found that the TOA pdf of GPS multipaths varies with the satellite elevation angle and that the probability of receiving very short-delay multipaths is much higher than receiving mid- or long-delay multipaths for all satellite elevation angles in urban environments. Section III also

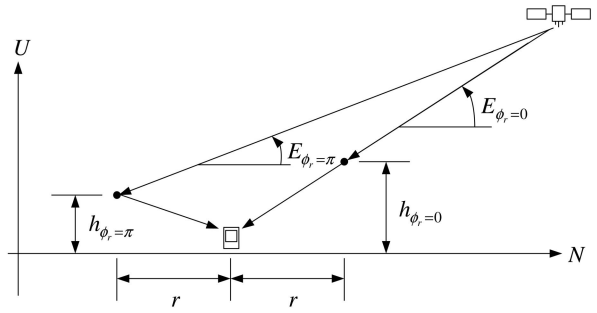

Fig. 1. Illustration of two multipaths arriving at GPS receiver.

includes comparisons of evaluated TOA pdfs to simulated normalized histograms obtained from numerous Monte Carlo trials of multipaths obtained from a 3-dimensional scatterer distribution. Based on the observations of Section III, Section IV analyzes the effect of the short-delay multipaths on conventional pseudo-range measurement functions, and some discussions and conclusions are provided in Section V.

II. MODELING SCATTERER DISTRIBUTION FOR URBAN GPS CHANNELS

A. Modeling Azimuthal Likelihood Distribution of Scatterers

Fig. 1 shows an example of two scatterers at azimuth angles $\phi_r = 0$ and $\phi_r = \pi$ producing multipaths of GPS signal transmitted from an azimuth angle $\phi_s = 0$ and a not very high elevation angle $E < 90°$. For the scatterer at ϕ_r, let L_{2,ϕ_r}, E_{ϕ_r}, and h_{ϕ_r} represent the distance from the satellite to the scatterer, the satellite elevation angle seen at the scatterer, and the height of the scatterer, respectively, in Fig. 1. It is assumed that multipaths reflected from the two scatterers maintain their propagation angle $E_{\phi_r=0}$ and $E_{\phi_r=\pi}$ as they arrive at the receiver. When the two scatterers are at the same horizontal distance r from the receiver,

$$2r = L_{2,\phi_r=\pi}\cos(E_{\phi_r=\pi}) - L_{2,\phi_r=0}\cos(E_{\phi_r=0}) \tag{1}$$

$$h_{\phi_r=0} - h_{\phi_r=\pi} = l(\tan(E_{\phi_r=0}) - \tan(E_{\phi_r=\pi})). \tag{2}$$

From (1),

$$\frac{2r}{L_{2,\phi_r=0}} = \frac{L_{2,\phi_r=\pi}}{L_{2,\phi_r=0}}\cos(E_{\phi_r=\pi}) - \cos(E_{\phi_r=0}). \tag{3}$$

Assuming $r < 10^4 m$ and $L_{2,\phi_r=\pi}/L_{2,\phi_r=0} \simeq 1$, it can be concluded that $2r/L_{2,\phi_r=0} \simeq 0$, and therefore

$$h_{\phi_r=0} \simeq h_{\phi_r=\pi} \tag{4}$$

$$E_{\phi_r=0} \simeq E_{\phi_r=\pi} \tag{5}$$

from (2) and (3), respectively. Note that $h_{\phi_r=0} = \max\{h_{\phi_r}\}$ and $h_{\phi_r=\pi} = \min\{h_{\phi_r}\}$, and (4) loses validity for its very high elevation angle. Therefore we assume

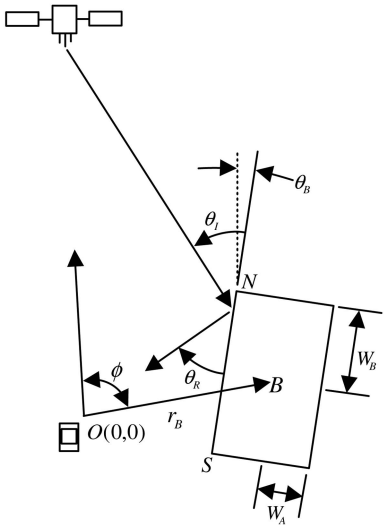

Fig. 2. Illustration of multipath arriving at GPS receiver.

that (4) holds for elevation angles $E < 90°$ and that the azimuthal likelihood distribution of scatterers is independent of the elevation angle E. Since the majority of scatterers for GPS signals in urban environments are buildings or solid objects, it can be assumed that GPS signals diffracted at or penetrated into the scatterers experience larger path loss than when reflected from the scatterers. Assuming large buildings and objects are uniformly distributed over all azimuth angles around the receiver, we can further assume that the probability of receiving an LOS path is negligible and that the probability density of receiving multipaths decreases as the relative azimuth angle decreases in dense urban environments. The likelihood distribution of relative azimuth angles of scatterers obtained from field measurements [3] shows similar properties to the above assumptions. Fig. 2 illustrates a situation where a multipath is reflected from a building (or object) at B which is at a distance r_B from a GPS receiver at the origin $O(0,0)$ on a horizontal plane. The GPS satellite and the building have azimuth angles ϕ_S and ϕ_B, respectively, and $\phi = |\phi_S - \phi_B|$ is the relative azimuth angle. The GPS signal is reflected from a building surface between the Northwest corner N and the Southwest corner S of the building, and the angles θ_I, θ_R $(= \theta_I)$ and θ_B represent the incidence angle and the reflection angle of the GPS signal and the building orientation in azimuth, respectively. Denoting θ_B^N and θ_B^S as the building orientation angles at which the reflection occurs at the building corners N and S, respectively, the coordinates of the building corners can be expressed as

$$\begin{aligned} N(\theta_B^N) &= (x_N, y_N)^T \\ &= B + T(\theta_B^N)(-W_A, W_B)^T \end{aligned} \tag{6}$$

$$\begin{aligned} S(\theta_B^S) &= (x_S, y_S)^T \\ &= B + T(\theta_B^S)(-W_A, -W_B)^T \end{aligned} \tag{7}$$

where

$$B = (r_B \sin(\phi_B), r_B \cos(\phi_B))^T \tag{8}$$

$$T(\theta_B) = \begin{bmatrix} \cos(\theta_B) & \sin(\theta_B) \\ -\sin(\theta_B) & \cos(\theta_B) \end{bmatrix} \tag{9}$$

and $2W_A$ and $2W_B$ are the depth and width of the building, respectively. After algebraic manipulations, it can be found that

$$\theta_B^N = \frac{1}{2}\left(\arctan\left(\frac{x_N}{y_N}\right) + \phi_S\right) \tag{10}$$

$$\theta_B^S = \frac{1}{2}\left(\arctan\left(\frac{x_S}{y_S}\right) + \phi_S\right). \tag{11}$$

Therefore there can be a multipath reflected from the building surface and arriving at the GPS receiver when

$$\min\{\theta_B^N, \theta_B^S\} \le \theta_B \le \max\{\theta_B^N, \theta_B^S\} \tag{12}$$

and it can be found that the difference between $\min\{\theta_B^N, \theta_B^S\}$ and $\max\{\theta_B^N, \theta_B^S\}$ is increasing as ϕ increases. Since the relative azimuth angle ϕ and the building orientation angle θ_B can be assumed uniformly distributed over $[0, 2\pi)$ and $[\phi, \phi + \pi)$, respectively, in a statistical viewpoint it is obvious that a building at larger ϕ has higher probability of producing a multipath to the GPS receiver. Assuming the GPS signal becomes too weak to be detected when the building (or object) completely blocks the satellite (i.e., $\phi = 0$), Fig. 3 shows the azimuthal likelihood distribution of scatterers obtained from computer calculation of (12). The simulation results show that the azimuthal likelihood distribution of scatterers increases with respect to ϕ. Note that the simulation results in Fig. 3 are from the assumption that buildings and objects are square in shape. Intuitively the azimuthal likelihood distribution of scatterers becomes uniform for $0 < \phi \le \pi$ when buildings and objects are circular in shape. However in practice there exist square and circular shaped buildings or objects around a GPS receiver, and therefore the azimuthal likelihood distribution of scatterers can have slightly larger density at low ϕ angles and slightly smaller density at high ϕ angles than the simulation results in Fig. 3 including the following general assumptions.

1) The effective antenna pattern of a GPS receiver is omnidirectional.

2) Each individual multipath that arrives at the receiver has interacted with only one scatterer in the channel.

3) The GPS receiver is at the ground level, and scatterers are above the ground level. The azimuthal likelihood distribution of scatterers can be modeled as

$$f_\phi(\phi) = \begin{cases} \dfrac{k}{2\pi}, & \phi_T < |\phi| \le \pi \\ \dfrac{k[\xi + \sin(\alpha|\phi|)]}{2\pi(1+\xi)}, & |\phi| \le \phi_T \end{cases} \tag{13}$$

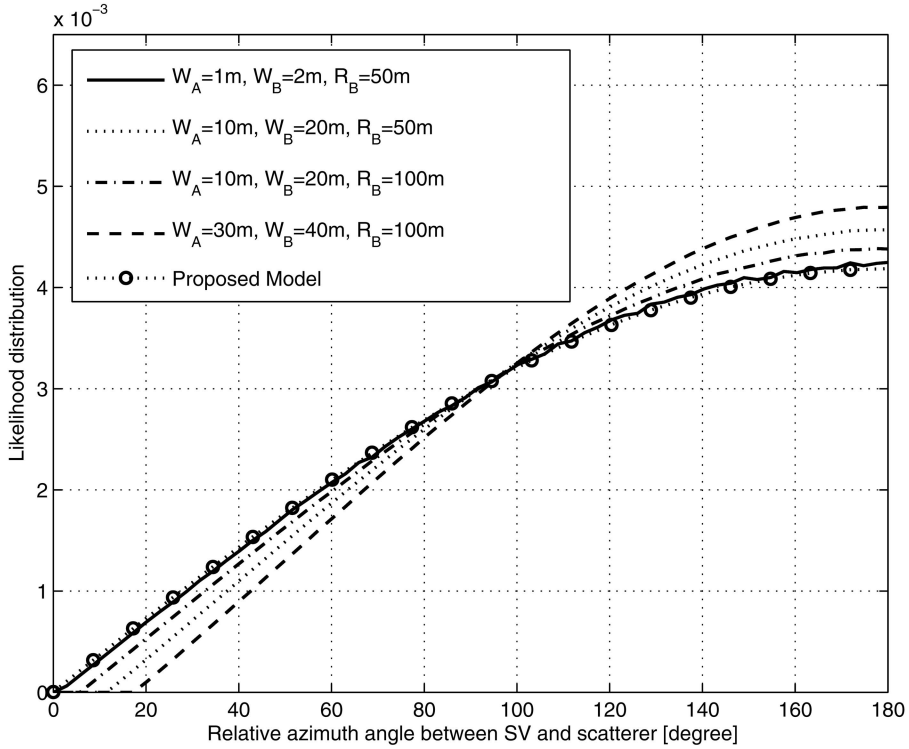

Fig. 3. Azimuthal likelihood distribution of scatterers.

where $\phi = \phi_r - \phi_s$, $0 \le \xi < 1$, $\alpha = \pi/2\phi_T$, $0 < \phi_T < \pi$, and k is a constant that normalizes $f_\phi(\phi)$

$$k = \frac{\pi\alpha(1+\xi)}{\alpha(\pi - \phi_T + \pi\xi) + 1 - \cos(\alpha\phi_T)}. \tag{14}$$

Since ξ is related to the probability density of receiving an LOS path in urban environments, we can assume that $\xi \simeq 0$ in dense urban environments. Note that (13) assumes $f_\phi(\phi)$ increases as $|\phi|$ increases from 0 to π. Note also that the required height for a building or an object around the receiver to be a scatterer decreases as $|\phi|$ increases from $|\phi| = 0$ to $|\phi| = \pi$, but the difference of the required height at $|\phi| = 0$ and $|\phi| = \pi$ is negligible when the elevation angle E is not very high as assumed in (4). Fig. 3 also shows $f_\phi(\phi)$ (13) for $\xi = 0$ and $\phi_T = \pi$. Since there exist wide buildings as well as narrow objects producing multipaths to a GPS receiver in urban environments, the azimuthal distribution of scatterers in very dense urban environment can be a weighted sum of the simulated likelihood distributions in Fig. 3, and $f_\phi(\phi)$ (13) agrees well with the simulation results in Fig. 3. Therefore we assume that (13) is valid when E is not very high.

B. Circular Gaussian Distribution of Scatterers

When a GPS receiver is at the ground level, any nearby building or object with height h at horizontal distance r from the receiver can be a scatterer producing a multipath to the receiver if $h \ge r\tan(E)$. Therefore the probability of any building or object with height h at horizontal distance r from the receiver being a scatterer can be expressed as

$$f_{r|E}(r \mid E) = \mathrm{P}\{h \ge r\tan(E)\}. \tag{15}$$

If we assume that the heights of buildings or objects follow normal distribution with non-zero mean H_s and variance σ_s^2 such that

$$h \sim N(H_s, \sigma_s^2) \tag{16}$$

then $f_{r|E}(r \mid E)$ in (15) decreases with r and has a narrower distribution for the higher elevation angle E. In [7] and [8], it is proposed that a circular Gaussian distribution model of scatterers is valid in a practical sense when the transmitter is well above the buildings or objects around the wireless receiver on the ground since the probability of a building (or an object) around the receiver being a scatterer producing a multipath to the receiver is higher than the probability of this occurring for a building (or an object) at a farther distance. In addition [2] shows that when scatterers are projected onto the horizontal plane, the probability density of projected scatterers decreases generally as the distance between the GPS receiver and scatterer increases. Therefore without loss of generality, we assume that the projected probability distribution of scatterers onto the horizontal plane can be approximated by circular Gaussian. Fig. 4 shows an illustration of a scatterer at an arbitrary location in the ENU (East-North-Up) coordinate system. A GPS receiver is located at the origin, the scatterer is located at $(r\sin(\phi_r), r\cos(\phi_r), r\tan(E))$ from the receiver, and a GPS satellite is located at $(L\cos(E)\sin(\phi_s), L\cos(E)\cos(\phi_s), L\sin(E))$, where E is the satellite elevation angle, r is the horizontal distance from the receiver to the projected scatterer location onto the horizontal plane, L is the LOS path length, and ϕ_r and ϕ_s are the azimuth angles of the scatterer and the satellite, respectively. The quantities L_2 and L_1 represent the propagation distance of the GPS signal from the satellite to the scatterer and that from the scatterer to the receiver, respectively. From (5), L_2 in Fig. 4 can be expressed using a linear approximation

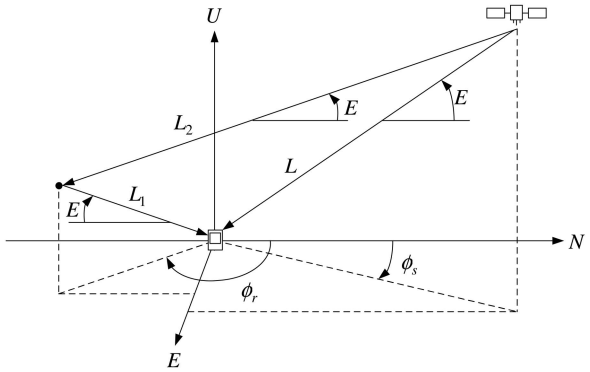

Fig. 4. Illustration of multipath arriving at GPS receiver.

$$\begin{aligned} L_2 &= \sqrt{L^2 + L_1^2 - 2Lr[\cos(E)\cos(\phi) + \sin(E)\tan(E)]} \\ &\simeq \sqrt{L^2 + L_1^2} - \frac{Lr[\cos(E)\cos(\phi) + \sin(E)\tan(E)]}{\sqrt{L^2 + L_1^2}} + \beta_1 \\ &\simeq L - r[\cos(E)\cos(\phi) + \sin(E)\tan(E)] + \beta_2 \end{aligned} \tag{17}$$

where β_1 and β_2 represent the sum of second-order or higher order terms in the linear approximation. Denoting t and τ as TOA and the excess delay of the received multipath, respectively,

$$\begin{aligned} \tau c &= tc - L \\ &= r\sec(E) - r[\cos(E)\cos(\phi) + \sin(E)\tan(E)] + \beta_2 \end{aligned} \tag{18}$$

where c is the speed of light. Since $\tau = 0$ for $\phi = 0$, $\beta_2 = r[\cos(E) + \sin(E)\tan(E) - \sec(E)]$, and therefore (18) becomes

$$\tau c = r\cos(E)[1 - \cos(\phi)] \tag{19}$$

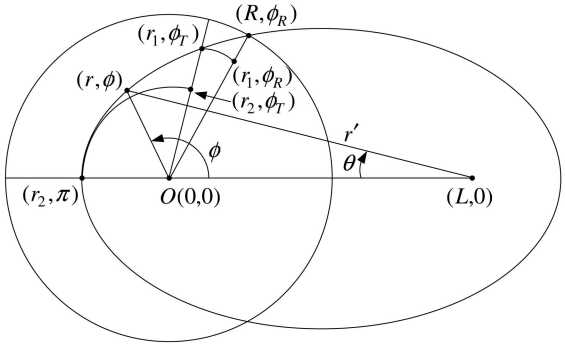

Fig. 5. Geometry of GPS scatterer distribution and area segments for TOA cdf.

where $0 < \phi < 2\pi$. From (19), since $tc \simeq L$ and $L \gg \tau c$,

$$\begin{aligned} r\cos(E) &\simeq \frac{\tau cL}{tc - L\cos(\phi)} \\ &\simeq \frac{(tc-L)L}{tc - L\cos(\phi)} \\ &\simeq \frac{(tc-L)(tc+L)}{2[tc - L\cos(\phi)]}. \end{aligned} \tag{20}$$

Equation (20) describes an ellipse [9] with its foci at $(0,0)$ and $(L,0)$, and any point on the ellipse can be defined by $(r\cos(E),\phi)$ in a polar coordinate system. Fig. 5 illustrates the ellipse in a polar coordinate system where

$$l = r\cos(E). \tag{21}$$

Note that (21) shows the effect of the elevation angle E on the size of the ellipse in terms of l; a scatterer at horizontal distance r from the receiver is on an ellipse with smaller l for a satellite with higher elevation angle. This observation agrees with the general property of $f_{r|E}(r \mid E)$ observed from (15) and (16). Therefore assuming σ_0 is the value of the standard deviation of the circular Gaussian scatterer distribution for GPS signals with elevation angle E_0 (≥ 0), the standard deviation σ of a circular Gaussian scatterer distribution for GPS signals with elevation angle E can be modeled as

$$\sigma = \frac{\sigma_0 \cos(E)}{\cos(E_0)}. \tag{22}$$

The standard deviation σ denotes the severeness of the multipath environment such that larger σ represents, intuitively, larger H_s or larger σ_s in (16).

C. Effective 2-Dimensional Scatterer Distribution Model for Urban GPS Signals

In Fig. 5, a receiver and a GPS satellite are located at the origin $O(0,0)$ and at $(L,0)$, respectively. An NLOS path with an angle of departure (AOD) θ relative to the LOS path is reflected from a scatterer at (r,ϕ) and arrives at the receiver with an angle of arrival (AOA) ϕ relative to the LOS path, after propagating TOA $t = (r + r')/c$ seconds where r' is the distance from the satellite to the scatterer. Assuming an x-y coordinate system is defined at the same origin O (x axis is $\phi = 0$); then $x = r\cos(\phi)$, $y = r\sin(\phi)$, and

$$r' = \frac{t^2c^2 - L^2}{2(tc - L\cos(\theta))}. \tag{23}$$

Denoting $f_{x,y}(x,y)$ as the circular Gaussian probability distribution of the scatterers within a circular scattering region, it can be expressed as

$$f_{x,y}(x,y) = \begin{cases} \dfrac{1}{2\pi\sigma^2}\exp\left[-\dfrac{x^2+y^2}{2\sigma^2}\right], & \sqrt{x^2+y^2} \leq R \\ 0, & \text{otherwise} \end{cases} \tag{24}$$

where R is the distance at which the density $f_{x,y}(x,y)$ becomes negligible. From (24), the radial distribution of scatterers $f_{r|E}(r \mid E)$ can be expressed by a Rayleigh distribution such that

$$f_{r|E}(r \mid E) = \frac{r}{\sigma^2}\exp\left[-\frac{r^2}{2\sigma^2}\right], \qquad r \geq 0 \tag{25}$$

where σ is defined in (22). Combining $f_\phi(\phi)$ (13) and $f_{r|E}(r \mid E)$ (25), a 2-dimensional scatterer distribution for an urban GPS signal with satellite elevation angle E can be expressed as

$$\begin{aligned} &f_{r,\phi|E}(r,\phi \mid E) \\ &= \begin{cases} \dfrac{kr}{2\pi\sigma^2}\exp\left[-\dfrac{r^2}{2\sigma^2}\right], & \\ \qquad\qquad r \leq R \quad \text{and} \quad \phi_T < |\phi| \leq \pi & \\ \dfrac{kr[\xi + \sin(\alpha|\phi|)]}{2\pi\sigma^2(1+\xi)}\exp\left[-\dfrac{r^2}{2\sigma^2}\right], & \\ \qquad\qquad r \leq R \quad \text{and} \quad |\phi| \leq \phi_T & \\ 0, \qquad\qquad \text{otherwise} \end{cases} \end{aligned} \tag{26}$$

where k, ξ, α, and ϕ_T are defined in (13) and σ is defined in (22). Note that (26) is valid when the satellite elevation angle E is not very high as discussed in Section IIA. Using a Jacobian transformation, [8–10] obtain expressions of the joint TOA/AOD probability density function (pdf) of cellular downlink channel for the circular scatterer distribution model, and the probability density of LOS path is obtained in [8]. Applying (13) to the probability density of receiving an LOS path in the 2-dimensional circular Gaussian scatterer distribution [8], the probability of receiving an LOS signal of a GPS satellite at elevation angle E can be expressed as

$$f_{t,\theta|E}(L/c, 0 \mid E) = \frac{k\xi cL}{2\pi\sigma^2(1+\xi)}. \tag{27}$$

III. MULTIPATH DELAY DISTRIBUTION OF URBAN GPS CHANNELS

The TOA pdf can be obtained by taking the derivative of the TOA cumulative density function

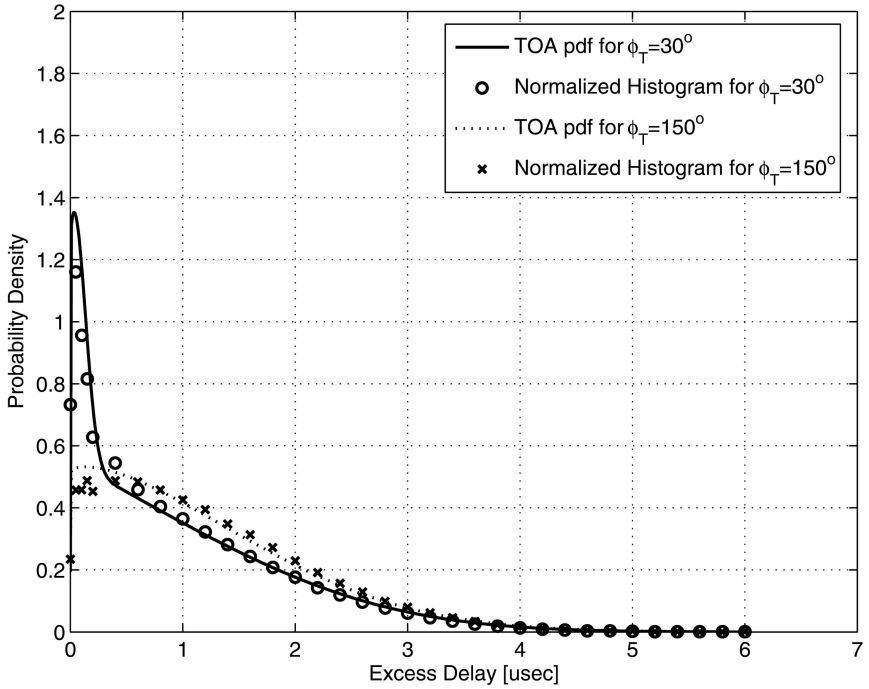

Fig. 6. TOA pdf for $E = 40°$ and $\phi_T = 30°$ and 150°.

(cdf) with respect to the TOA t, and the TOA cdf can be obtained by evaluating the total probability of a scatterer inside both the ellipse corresponding to a delay equal to t and the circular scattering region of radius R [9] in Fig. 5. Similarly to the algebraic approaches used in [9] and [8], the intersection area can be divided into multiple area segments so that the TOA cdf can be obtained from the sum of probability masses over the area segments. Fig. 5 illustrates the area segments considered for TOA cdf calculation. Due to the symmetry of the scatterer distribution, only segments for $0 \le \phi \le \pi$ are depicted in detail and analyzed for algebraic convenience. An arbitrary point inside the intersection area is represented by a radius r from a GPS receiver located at the origin $O(0,0)$ and an angle ϕ increasing counterclockwise from the AOA of the LOS path of the GPS satellite at $(L,0)$. For a TOA t, ϕ_R represents the angle to the cross-section point of the circle and the ellipse, and r_2 is the distance from the origin to a point on the ellipse when $\phi = \pi$, i.e., $r_2 = (tc - L)/2$. The complete expression of the TOA pdf can be expressed as

$$f_{t|E}(t \mid E) = \begin{cases} f^1_{t|E}(t \mid E), & t_T < t \le t_{\max} \\ f^2_{t|E}(t \mid E), & t_{\min} < t \le t_T \\ \dfrac{k\xi cL}{2\pi\sigma^2(1+\xi)}, & t = t_{\min} \\ 0, & \text{otherwise} \end{cases} \tag{28}$$

where $f^1_{t|E}(t \mid E)$ and $f^2_{t|E}(t \mid E)$ are defined in the Appendix. Note that the probability density at LOS ($t = t_{\text{LOS}}$) in (28) is obtained from

$$f_{t|E}(L/c \mid E) = \int_0^{2\pi} f_{t,\theta|E}(L/c, \theta \mid E) d\theta = f_{t,\theta|E}(L/c, 0 \mid E) \tag{29}$$

which is derived in (27). Note that the closed-form expression of the TOA pdf (28) loses validity for very small or very large ϕ_T due to approximation error in (53). To test the validity of the closed-form expression of the TOA pdf in (28), both Fig. 6 and Fig. 7 show TOA pdfs, when $L = 20200$ km, $R = 300$ m, $\sigma_0 = 300$ m, $\phi_T = 90°$, and $\xi = 10^{-5}$ are assumed, and the simulated normalized histograms of TOAs obtained from 10^5 Monte Carlo trials are shown for comparisons. Fig. 6 shows TOA pdfs obtained from (28) and simulated normalized histograms for two ϕ_T values, 30° and 150° when $E = 40°$. And Fig. 7 shows TOA pdfs obtained from (28) and simulated normalized histograms for three GPS satellite elevation angles $E = 70°$, 40°, and 10°, when $\phi_T = 90°$. The Monte Carlo trials, for simulated normalized histograms of TOAs in Fig. 6 and Fig. 7 assume that scatterers are due to tall enough buildings or objects satisfying (15) and that their projected likelihood distribution onto the horizontal plane follows (26). Note that ξ is assumed negligible since the combined scatterer distribution model (26) assumes buildings and objects are at all azimuth directions from the receiver so that the probability of having an LOS path in an urban area is negligible. As shown the probability density of TOA decreases as the excess delay τ increases in all

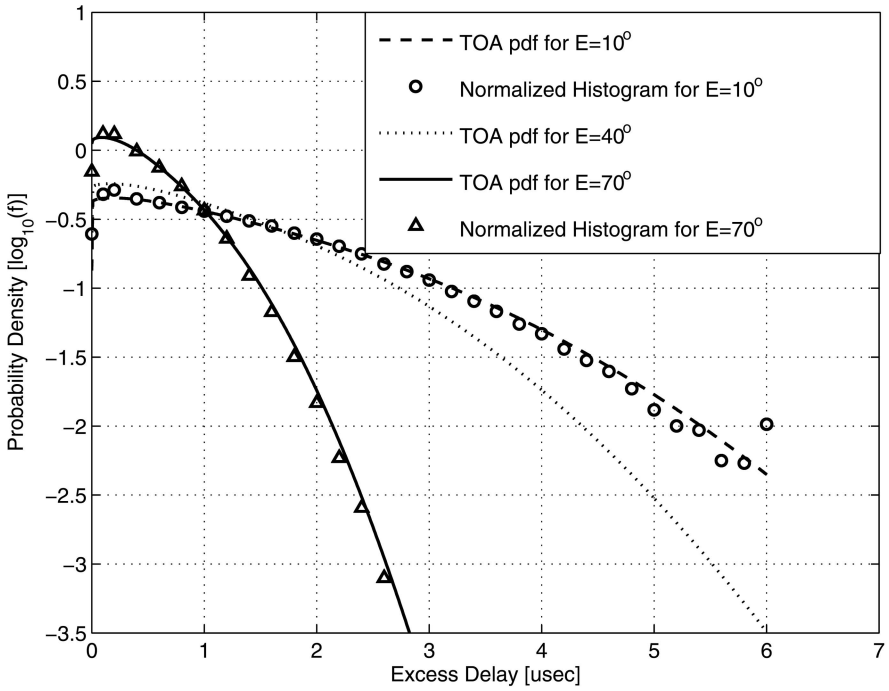

Fig. 7. TOA pdf for $\phi_T = 90°$ and $E = 70°$, $40°$, and $10°$.

elevation angles, and it decreases faster for higher SV elevation angles for $\tau > 0$ so that the TOA pdf has narrower distribution for higher elevation angle. Note that the changes in TOA pdfs shown in Fig. 7 with the GPS elevation angle E are very similar to field observations in [3]. In addition from Figs. 6 and 7, we can observe that short-delay multipaths occur with much higher probability than mid- or long-delay multipaths so that they often become a cause of pseudo-range measurement errors in urban environments.

IV. SHORT-DELAY MULTIPATH

It is well known that the pseudo-range measurement from a detected and resolved first arrival path can be much different from that from the true first arrival path if there is sufficiently strong short-delay multipaths. In [4], [5] and [6], pseudo-range measurement errors due to the short-delay multipaths are studied for conventional early-late correlator-based code phase measurement functions. The above papers show that the pseudo-range measurement error has symmetric distribution when the later arrival path has smaller strength than the first arrival path. The papers also show that the peak detection performance can be improved by narrower correlator spacing, in general, and that the effect of the noise on the peak detection is reduced with increased signal-to-noise ratio (SNR). Therefore the effect of short-delay multipaths on the pseudo-range measurement error can be small or negligible when the LOS path is present since the LOS path is much stronger than any other multipaths. As we observed from Section III, a sufficient probability of having short-delay multipaths exists in urban environments. In addition $f_{r,\phi|E}(r,\phi \mid E)$ in (28) shows that the scatterers producing very short-delay multipaths are reflectors close to the receiver and that the probability of receiving an LOS path in an urban environment is very small. Therefore the short-delay multipaths can have relatively strong signal strengths compared with the first arrival path that might not be the LOS. In [11], pseudo-range measurement errors due to a short-delay multipath are studied based on an assumption of an ideal triangular shape autocorrelation function. However, the code phases of the true first arrival path and the short-delay multipaths are very close each other and also very close to the code phase of the resolved path. The pseudo-range measurement errors due to the short-delay multipaths can be significant when the correlation output has round shape peak as is common to most GPS receivers with bandlimited filters. This section focuses on the statistical analysis of pseudo-range measurement errors due to the short-delay multipaths for conventional GPS code phase measurement functions with bandlimited filters. The analysis of pseudo-range measurement errors related to the correlator spacing and noise input are not included in this section.

A. Coherent Code Phase Measurement

Fig. 8 shows a simplified diagram of a coherent code phase measurement function used for a conventional coherent delay lock loop (DLL) discriminator in GPS receivers. The received GPS

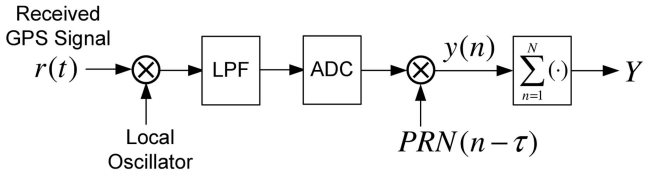

Fig. 8. Coherent code phase measurement function.

signal $r(t)$ is first multiplied by a locally generated carrier. Since we are interested in the code phase measurement errors in the GPS receiver after signal acquisition state, we assume the locally generated carrier wave is perfectly aligned with the estimated carrier wave from the detected and resolved first arrival path. Afterwards the signal passes through a low pass filter (LPF) and an analogue-to-digital converter (ADC) to yield a baseband input signal. The baseband input signal is then multiplied by a locally generated GPS psuedorandom noise (PRN) sequence in which the code phase is delayed by τ to match the code phase delay of the detected and resolved first arrival path. Note that no error is assumed in detecting the peak position of the detected and resolved first arrival path. We also assume that there are $M(>1)$ unresolvable multipaths and a true first arrival path constituting the detected and resolved first arrival path. We denote $\alpha_m(t)$ as the amplitude of the mth $(1 < m \le M+1)$ multipath and $\psi_m(t)$ as the phase difference between the mth multipath carrier and the locally generated carrier, such that

$$\psi_m(t) = 2\pi(f_c - f_{D_m}(t))\tau_m(t) + \psi_{0_m} \tag{30}$$

where f_c, $f_{D_m}(t)$, $\tau_m(t)$, and, ψ_{0_m} are the carrier frequency, Doppler frequency, code phase delay, and an unknown random phase offset, respectively; $y(n)$ is coherently accumulated for N chips to yield correlator output $Y(\tau)$. Assuming that the amplitude $\alpha_m(n)$, code phase delay $\tau_m(n)$, and Doppler frequency $f_{D_m}(n)$ are changing slowly enough to be considered constant over the N chip correlation length, $Y(\tau)$ can be expressed as

$$Y(\tau) = N\sum_{m=1}^{M}\alpha_m R(\tau-\tau_m)\cos(\psi_m) + \sum_{n=1}^{N} n_t(n) \tag{31}$$

where $R(\tau-\tau_m)$ is the autocorrelation function between the C/A code of the mth multipath component, and the locally generated C/A code has a code phase delay τ; n_t is an additive white Gaussian noise (AWGN) process with one-sided power spectral density N_0. The assumption used for (31) is valid when each of the multipath components is associated with a single scatterer [12]. The autocorrelation function has a round shape peak due to the bandlimited filter used in the receiver. In general narrower filter brandwidths tend to make the autocorrelation peak more rounded. Since $|\tau-\tau_m|$ is very small, one of the effective models representing the round peak of $R(\tau-\tau_m)$ can be

$$R(\tau-\tau_m) \simeq \frac{\sin(\pi\Delta_m)}{\pi\Delta_m} \tag{32}$$

where $\Delta_m = \tau-\tau_m$. Note that the approximation (32) is not general for GPS receivers with a wide bandwidth filter. However most of the GPS receivers without very wide bandwidth filters have a round autocorrelation peak over $[-\epsilon,\epsilon]$ from the center, where ϵ varies inversely proportional to the bandwidth. Assuming ϵ is not very small and the very short-delay multipaths are within $[0,\epsilon]$, the approximation (32) is valid for GPS receivers with narrow bandwidth filter. A coherent DLL discriminator compares $Y^-(\tau)$ and $Y^+(\tau)$ which are the correlation outputs of the function shown in Fig. 8 at δ chip early and δ chip late code phases, respectively. Usually, δ is chosen 0.5 chips or less. When the short-delay multipaths are arriving close to each other such that

$$|\tau_i-\tau_j| \ll 1 \qquad \text{for} \quad 1<i, \quad j \le M+1 \tag{33}$$

the sum of short-delay multipath arrivals can be effectively approximated by a single short-delay multipath arrival, and therefore (31) can be approximated as

$$Y(\tau) \simeq N\alpha_1 R(\tau-\tau_1)\cos(\psi_1) + N\alpha_t R(\tau-\tau_t)\cos(\psi_t) + \sum_{n=1}^{N} n_t(n) \tag{34}$$

where α_t, τ_t, and ψ_t represent the amplitude, code phase delay, and carrier phase of the short-delay multipath, which is the sum of short-delay multipaths. We can further assume that $\tau_t-\tau_1 \ll 1$ for the short-delay multipaths, and we can use the Taylor series of (32) to find the code phase delay of the detected and resolved path τ from (34);

$$\begin{aligned}\frac{\partial Y(\tau)}{\partial\tau} &\simeq N\alpha_1\cos(\psi_1)\frac{\partial}{\partial\tau}\sum_{k=0}^{\infty}\frac{(-\pi^2\Delta_1^2)^k}{(2k+1)!} \\ &\quad + N\alpha_t\cos(\psi_t)\frac{\partial}{\partial\tau}\sum_{k=0}^{\infty}\frac{(-\pi^2\Delta_t^2)^k}{(2k+1)!} + \frac{\partial}{\partial\tau}\sum_{n=1}^{N} n_t(n) \\ &\approx \frac{-\pi^2}{3}N[\alpha_1\cos(\psi_1)(\Delta_1) + \alpha_t\cos(\psi_t)(\Delta_t)] \\ &= 0\end{aligned} \tag{35}$$

where Δ_1 and Δ_t denote $\tau-\tau_1$ and $\tau-\tau_t$, respectively. From (35) the code phase delay of the detected and resolved first arrival path is

$$\tau \approx \frac{\alpha_1\cos(\psi_1)\tau_1 + \alpha_t\cos(\psi_t)\tau_t}{\alpha_1\cos(\psi_1) + \alpha_t\cos(\psi_t)} \tag{36}$$

and therefore the pseudo-range measurement error τ_e is

$$\begin{aligned}\tau_e^C &= \tau - \tau_1 \\ &\approx \frac{\alpha_t \cos(\psi_t)(\tau_t - \tau_1)}{\alpha_1 \cos(\psi_1) + \alpha_t \cos(\psi_t)}\end{aligned} \tag{37}$$

where the superscript $(\cdot)^C$ represents coherent code phase measurement. Intuitively $\psi_1 \to 0$ and ψ_t can be assumed to be random and uniformly distributed on $[-\pi, \pi]$ when $|\alpha_1|$ increases larger than $|\alpha_t|$ since the true first arrival path dominates the detected and resolved first arrival path. On the other hand $\psi_t \to 0$ and ψ_1 can be assumed to be random and uniformly distributed on $[-\pi, \pi]$ when $|\alpha_1|$ decreases smaller than $|\alpha_t|$, since the short-delay multipaths dominate the detected and resolved first arrival path. Therefore

$$\tau_e^C \approx \begin{cases} \dfrac{\alpha_t \cos(\psi_t)(\tau_t - \tau_1)}{\alpha_1 + \alpha_t \cos(\psi_t)}, & \text{for} \quad |A_r| \gg 1 \\ \dfrac{\alpha_t (\tau_t - \tau_1)}{\alpha_1 \cos(\psi_1) + \alpha_t}, & \text{for} \quad |A_r| \ll 1 \\ \dfrac{\alpha_t \cos(\psi_t)(\tau_t - \tau_1)}{\alpha_1 \cos(\psi_1) + \alpha_t \cos(\psi_t)}, & \text{otherwise} \end{cases} \tag{38}$$

where $A_r = \alpha_1/\alpha_t$. In rural environments where $|A_r| \gg 1$, (38) indicates that τ_e^C can be negative or positive depending on ψ_t as studied in [4], [5], and [6], and $E[\tau_e^C] \to 0$ as $|A_r|$ increases. In NLOS environments such as dense urban and indoor areas where $|A_r| \ll 1$, τ_e^C can always be positive and $E[\tau_e^C] \to (\tau_t - \tau_1)$ as $|A_r|$ decreases. In many multipath environments, however, $|A_r|$ can be neither very small nor large enough so that τ_e^C can change rapidly even for a small value of $\tau_t - \tau_1$. In this case code tracking using the coherent DLL discriminator may fail or result in a large pseudo-range measurement error. Since τ_e^C in (38) is proportional to $\tau_t - \tau_1$ in a given multipath environment and τ_t has wider distribution for lower satellite elevation angle E as expressed in (28), it is expected that the distribution of τ_e^C is wider for lower E.

B. Noncoherent Code Phase Measurement

Fig. 9 shows a simplified diagram of a noncoherent code phase measurement function used for a noncoherent DLL discriminator in conventional GPS receivers. The received GPS signal $r(t)$ is first multiplied by a locally generated carrier wave. The multiplication with the locally generated carrier wave generates an in-phase signal, and multiplication with a 90° phase-shifted version of the locally generated carrier wave generates quadrature-phase signal. Both in-phase and quadrature-phase signals pass through an LPF and an ADC to yield baseband sampled signals

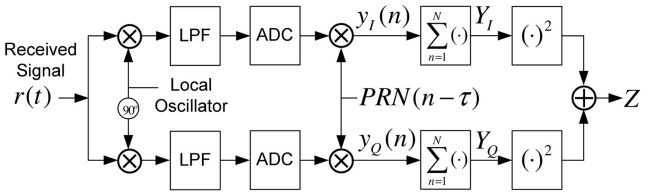

Fig. 9. Noncoherent code phase measurement function.

in both in-phase and quadrature-phase arms. Both baseband sampled signals are then multiplied by a locally generated GPS PRN code sequence of which the code phase is delayed by τ to match the code phase of the detected and resolved first arrival path. Applying the same assumptions and notations used to derive (31) and (34), approximate expressions of intermediate in-phase and quadrature-phase measurements $Y_I(\tau)$ and $Y_Q(\tau)$ can be expressed as

$$\begin{aligned}Y_I(\tau) &\simeq N\alpha_1 R(\tau - \tau_1)\cos(\psi_1) + N\alpha_t R(\tau - \tau_t)\cos(\psi_t) \\ &\quad + \sum_{n=1}^{N} n_I(n)\end{aligned} \tag{39}$$

$$\begin{aligned}Y_Q(\tau) &\simeq N\alpha_1 R(\tau - \tau_1)\sin(\psi_1) + N\alpha_t R(\tau - \tau_t)\sin(\psi_t) \\ &\quad + \sum_{n=1}^{N} n_Q(n)\end{aligned} \tag{40}$$

where $n_I(n)$ and $n_Q(n)$ are independent AWGN processes, each with a one-sided power spectral density of $N_0/2$. From (39) and (40), the decision variable $Z(\tau)$ is expressed as

$$\begin{aligned}Z(\tau) &= Y_I(\tau)^2 + Y_Q(\tau)^2 \\ &\simeq N^2[\alpha_1^2 R(\Delta_1)^2 + \alpha_t^2 R(\Delta_t)^2] \\ &\quad + 2N^2\alpha_1\alpha_t R(\Delta_1)R(\Delta_t)\cos(\psi) + N_t\end{aligned} \tag{41}$$

where N_t represents the final noise term $\psi = \psi_1 - \psi_t$, and Δ_1 and Δ_t denote $\tau - \tau_1$ and $\tau - \tau_t$, respectively. The noncoherent DLL discriminator compares $Z^-(\tau)$ and $Z^+(\tau)$, which are the correlation outputs of the function shown in Fig. 9 at δ chip early and δ chip late code phases, respectively. Assuming $|\tau_t - \tau_1| \ll 1$, we can use the Taylor series of (32) to find the code phase delay τ of the detected and resolved path delay τ from (41)

$$\begin{aligned}\frac{\partial Z(\tau)}{\partial \tau} &\approx \frac{-2\pi^2}{3} N^2[\alpha_1^2 R(\Delta_1)\Delta_1 + \alpha_t^2 R(\Delta_t)\Delta_t \\ &\qquad + \alpha_1\alpha_t\cos(\psi)(R(\Delta_t)\Delta_1 + R(\Delta_1)\Delta_t)] \\ &\quad + \frac{\partial}{\partial \tau} N_t \\ &= 0.\end{aligned} \tag{42}$$

From (42) an approximate expression of the pseudo-range measurement error due to the

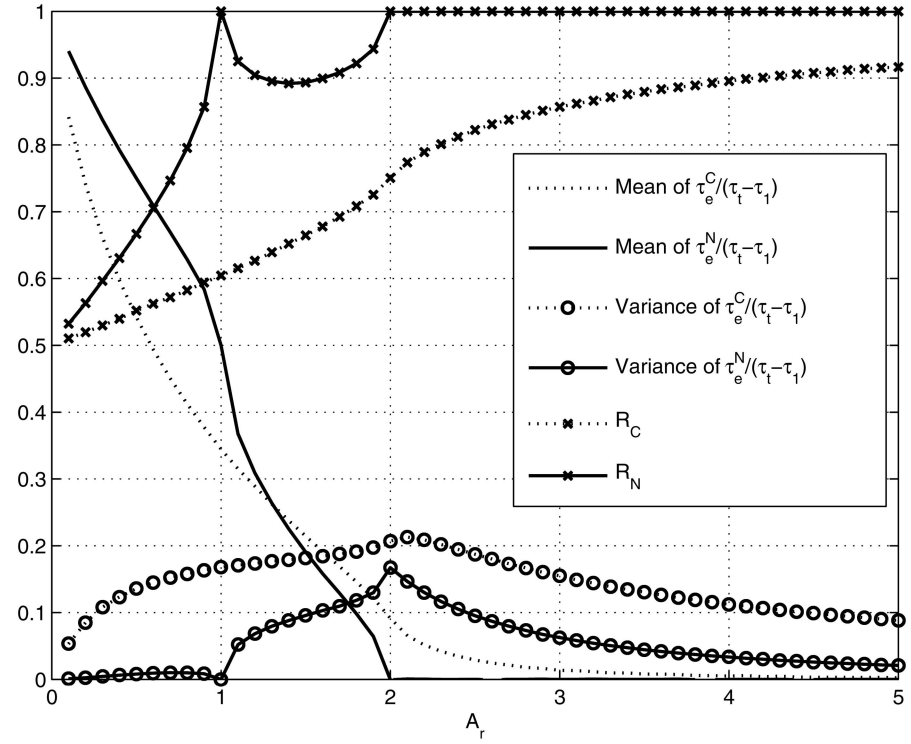

Fig. 10. Simulated mean and variance of τ_e^C and τ_e^N for $0 < |A_r| \le 5$.

short-delay multipaths can be derived as

$$\begin{aligned}\tau_e^N &= \tau - \tau_1 \\ &\approx \frac{[\alpha_t^2 R(\Delta_t) + \alpha_1\alpha_t\cos(\psi)R(\Delta_1)](\tau_t-\tau_1)}{\alpha_1^2 R(\Delta_1) + \alpha_t^2 R(\Delta_t) + \alpha_1\alpha_t\cos(\psi)[R(\Delta_1)+R(\Delta_t)]} \\ &\approx \frac{[\alpha_t^2 + \alpha_1\alpha_t\cos(\psi)](\tau_t-\tau_1)}{\alpha_1^2+\alpha_t^2+2\alpha_1\alpha_t\cos(\psi)} \end{aligned} \tag{43}$$

where the superscript $(\cdot)^N$ represents noncoherent code phase measurement function. With the same intuition used to derive (38),

$$\tau_e^N \approx \begin{cases} \dfrac{\alpha_t\cos(\psi)(\tau_t-\tau_1)}{\alpha_1+2\alpha_t\cos(\psi)}, & \text{for} \quad |A_r| \gg 1 \\ \dfrac{\alpha_t(\tau_t-\tau_1)}{2\alpha_1\cos(\psi)+\alpha_t}, & \text{for} \quad |A_r| \ll 1 \\ \dfrac{[\alpha_t^2+\alpha_1\alpha_t\cos(\psi)](\tau_t-\tau_1)}{\alpha_1^2+\alpha_t^2+2\alpha_1\alpha_t\cos(\psi)}, & \text{otherwise.} \end{cases} \tag{44}$$

For the LOS environment ($|A_r| \gg 1$), (44) indicates that τ_e^N can be negative or positive depending on ψ and $E[\tau_e^N] \to 0$ as $|A_r|$ increases. For NLOS environment with $A_r \ll 1$, τ_e^N is always positive, and $E[\tau_e^N] \to (\tau_t - \tau_1)$ as $|A_r|$ decreases. Therefore the performance of the noncoherent code phase measurement function is very similar to the coherent code phase measurement function for both $|A_r| \gg 1$ and $|A_r| \ll 1$ cases. However when $|A_r|$ is neither small nor large enough, the performance of the noncoherent code phase measurement function can be better than that of coherent code phase measurement function since the denominator of τ_e^C becomes zero whenever $\alpha_1\cos(\psi_1) = -\alpha_t\cos(\psi_t)$, but the denominator of τ_e^N becomes zero only when $\alpha_1 = \alpha_t$ and $\psi_1 - \psi_t = \pi$. The coherent code phase measurement function will have a large error more often than the noncoherent code phase measurement function. Note that the expressions in (38) and (44) are derived using the approximation of the autocorrelation function (32). Therefore depending on the roundness of the autocorrelation peak, a GPS receiver can have different performance in the presence of short-delay multipaths. We denote R_C and R_N as acceptable performance rates such that the coherent code phase measurement results in $|\tau_e^C| \le \tau_t - \tau_1$ and the noncoherent code phase measurement results in $|\tau_e^N| \le \tau_t - \tau_1$, respectively. Fig. 10 shows simulated performance of the code phase measurement functions in the presence of short-delay multipaths obtained from 10^6 Monte Carlo trials for $0.1 \le |A_r| \le 5$. The statistical values (mean and variance) of $\tau_e^C/(\tau_t - \tau_1)$ and $\tau_e^N/(\tau_t - \tau_1)$ are obtained from the results when the code phase measurement performance is acceptable. The acceptable performance rates R_C and R_N are also shown in Fig. 10. As expected $E[\tau_e^C]$ has a larger error than $E[\tau_e^N]$ when $|A_r| > 1.2$, and $\mathrm{Var}[\tau_e^C]$ is larger than $\mathrm{Var}[\tau_e^N]$ for $0.1 \le |A_r| \le 5$.

V. CONCLUSION

Based on geometrical scatterer distribution model that agrees with field observations introduced

by previous studies, TOA pdf of GPS multipaths in urban environments has been derived. It has been shown that the derived TOA pdf also agrees with field observations on the delay distribution of multipaths such that the TOA probability density decreases exponentially with multipath delay and that the TOA pdf becomes narrower as the GPS satellite elevation angle increases. However, the derived TOA pdf still needs complete verification with many field measurements from diverse urban environments, which may be an area for further study. From the derived TOA pdf, it has been shown that the probability density of short-delay multipaths is much higher than other later arrival multipaths in urban GPS environments, so the pseudo-range measurement errors due to the short-delay multipaths can be significant with conventional code phase measurement functions. From Monte Carlo simulations of coherent and noncoherent code phase measurement functions, it has been found that the noncoherent code phase measurement function has better performance in the presence of short-delay multipaths.

APPENDIX. DERIVATION OF TOA PDF

Let A_0 denote the total circular scattering region, and let A_1, A_2, A_3, A_4,and A_5 represent area segments which constitute the intersection area for $0 \le \phi < \pi$, over $\{0 \le \phi < \phi_R\}$, $\{0 \le r < r_2, \max\{\phi_T, \phi_R\} \le \phi < \pi\}$, $\{r_2 \le r < r_1, \max\{\phi_T, \phi_R\} \le \phi < \pi\}$, $\{0 \le r < r_1$, $\phi_R \le \phi < \max\{\phi_T, \phi_R\}\}$, and $\{r_1 \le r < R, \phi_R \le \phi < \max\{\phi_T, \phi_R\}\}$, respectively. The total probability mass over A_0 is

$$V_0 = \int_0^R \int_0^{2\pi} f_{r,\phi|E}(r, \phi \mid E) d\phi dr.$$
$$= 1 - \exp\left(\frac{-R^2}{2\sigma^2}\right) \quad (45)$$

where σ is defined in (22), and therefore $V_0 \simeq 1$ for $R \gg \sigma$, Since the distance from the origin to the ellipse corresponding to a TOA t is described by

$$r = \frac{t^2c^2 - L^2}{2(tc - L\cos(\phi))} \quad (46)$$

as in [9], the following relationships are obtained

$$\phi = \arccos\left(\frac{L^2 - t^2c^2 + 2rtc}{2rL}\right) \quad (47)$$

$$\phi_R = \arccos\left(\frac{L^2 - t^2c^2 + 2Rtc}{2RL}\right) \quad (48)$$

$$r_1 = \begin{cases} \dfrac{t^2c^2 - L^2}{2(tc - L\cos(\phi_T))}, & \phi_R < \phi_T \\ R, & \text{otherwise.} \end{cases} \quad (49)$$

Denoting the TOA values when $\phi_R = 0$, $\phi_R = \phi_T$, and $\phi_R = \pi$ by $t_{\min}$, t_T, and $t_{\max}$, respectively, it can be found from (46) that $t_{\min} = L/c$, $t_T = (R + \sqrt{R^2 - 2RL\cos(\phi_T) + L^2})/c$, and $t_{\max} = (L + 2R)/c$. When $t_T < t \le t_{\max}$, $V_4 = V_5 = 0$, and the probability mass over A_1 can be expressed as

$$V_1 = \frac{k}{2\pi}\left[\int_0^{\phi_T} \xi + \sin(\alpha\phi) d\phi + \int_{\phi_T}^{\phi_R} d\phi\right]$$
$$= \frac{k}{2\pi}\left[\phi_R + \frac{M_1}{\alpha(1+\xi)}\right] \quad (50)$$

where $M_1 = 1 - \alpha\phi_T - \cos(\alpha\phi_T)$. The probability masses over A_2 and A_3 for $t_T < t \le t_{\max}$ can be expressed by the following equations:

$$V_2 = \frac{k}{2\pi}\int_0^{r_2} (\pi - \phi_R) f_{r|E}(r \mid E) dr$$
$$= \frac{k}{2\pi}(\pi - \phi_R)\left[1 - \exp\left(\frac{-r_2^2}{2\sigma^2}\right)\right] \quad (51)$$

$$V_3 = \frac{k}{2\pi}\int_{r_2}^{R} (\phi - \phi_R)\frac{r}{\sigma^2}\exp\left(\frac{-r^2}{2\sigma^2}\right) dr. \quad (52)$$

Using first-order approximation

$$\arccos x \simeq \frac{\pi}{2} - x \quad (53)$$

and the same algebraic manipulation used in [8], the quantity $(\phi - \phi_R)r$ in (52) can be approximated as

$$(\phi - \phi_R)r \simeq \left(\frac{\pi}{2} - \phi_R - \frac{tc}{L}\right) r + \frac{r_2(tc + L)}{L}. \quad (54)$$

Denoting $M_2 = 1 - \exp(-r_2^2/(2\sigma^2))$ and $M_3 = r_2(tc + L)/L$, the quantity V_3 (52) can be expressed as

$$V_3 \simeq \frac{k}{2\pi}\left(\frac{\pi}{2} - \phi_R - \frac{tc}{L}\right)\left(1 - M_2 - \exp\left(\frac{-R^2}{2\sigma^2}\right)\right)$$
$$+ \frac{kM_3}{\sigma\sqrt{2\pi}}\left(Q\left(\frac{r_2}{\sigma}\right) - Q\left(\frac{R}{\sigma}\right)\right) \quad (55)$$

where

$$Q(x) = \frac{1}{\sqrt{2\pi}}\int_x^{\infty} e^{-t^2/2} dt.$$

Assuming $R \gg \sigma$, it can be found that $\exp(-R^2/(2\sigma^2)) \simeq 0$ and $Q(R/\sigma) \simeq 0$. After some algebraic manipulations the TOA cdf for $t_T < t \le t_{\max}$ can be expressed as

$$F_{t|E}^1(t \mid E) = 2(V_1 + V_2 + V_3)$$
$$\simeq \frac{k}{\pi}\left[\frac{\pi}{2} - \frac{tc}{L} + \left(\frac{\pi}{2} + \frac{tc}{L}\right)M_2 + \frac{M_1}{\alpha(1+\xi)}\right]$$
$$+ \frac{2kM_3}{\sigma\sqrt{2\pi}}Q\left(\frac{r_2}{\sigma}\right). \quad (56)$$

When $t_{\min} < t \le t_T$,

$$V_1 = \frac{k}{2\pi}\left[\int_0^{\phi_R} \xi + \sin(\alpha\phi) d\phi\right]$$
$$= \frac{k}{2\pi\alpha(1+\xi)}[\alpha\xi\phi_R + 1 - \cos(\alpha\phi_R)] \quad (57)$$

$$V_2 = \frac{k}{2\pi}\int_0^{r_2} (\pi - \phi_T) f_{r|E}(r \mid E) dr$$
$$= \frac{k}{2\pi}(\pi - \phi_T) M_2 \quad (58)$$

$$V_3 = \frac{k}{2\pi}\int_{r_2}^{r_1} (\phi - \phi_T)\frac{r}{\sigma^2}\exp\left(\frac{-r^2}{2\sigma^2}\right) dr$$
$$\simeq \frac{k}{2\pi}\left[\frac{\pi}{2} - \phi_T - \frac{tc}{L}\right](M_4 - M_2)$$
$$+ \frac{kM_3}{\sigma\sqrt{2\pi}}\left[Q\left(\frac{r_2}{\sigma}\right) - Q\left(\frac{r_1}{\sigma}\right)\right] \quad (59)$$

$$V_4 = \int_0^{r_1}\int_{\phi_R}^{\phi_T} f_\phi(\phi) f_{r|E}(r \mid E) d\phi dr$$
$$= \frac{kM_4}{2\pi\alpha(1+\xi)}[\alpha\xi(\phi_T - \phi_R) + \cos(\alpha\phi_R) - \cos(\alpha\phi_T)] \quad (60)$$

$$V_5 = \int_{r_1}^{R}\int_{\phi_R}^{\phi_T} f_\phi(\phi) f_{r|E}(r \mid E) d\phi dr \quad (61)$$

where $M_4 = 1 - \exp(-r_1^2/(2\sigma^2))$. Since $f_\phi(\phi_T) > f_\phi(\phi_R)$,

$$V_5 > f_\phi(\phi_R)\int_{r_1}^{R} (\phi - \phi_R) f_{r|E}(r \mid E) dr \quad (62)$$
$$< f_\phi(\phi_T)\int_{r_1}^{R} (\phi - \phi_R) f_{r|E}(r \mid E) dr. \quad (63)$$

Note that V_5 is negligible when t is large and $(\phi_T - \phi_R)$ is small for most of $r_1 < r \le R$ when t is small. Therefore as a rule of thumb, V_5 (61) can be approximated as

$$V_5 \simeq \frac{1}{2}(f_\phi(\phi_R) + f_\phi(\phi_T))\int_{r_1}^{R} (\phi - \phi_R) f_{r|E}(r \mid E) dr. \quad (64)$$

As shown in Fig. 5, $(\phi - \phi_R)r$ within the integral of (64) decreases from $(\phi_T - \phi_R)r_1$ to 0 as r increases from r_1 to R, and therefore $(\phi - \phi_R)r$ can be approximated by a first-order approximation

$$(\phi - \phi_R)r \simeq \frac{(\phi_T - \phi_R)r_1}{R - r_1}(R - r). \quad (65)$$

After some algebraic manipulations, an approximate expression for (64) can be obtained

$$V_5 \simeq \frac{1}{2}(f_\phi(\phi_R) + f_\phi(\phi_T))M_5\left[\frac{R\sqrt{2\pi}}{\sigma}Q\left(\frac{r_1}{\sigma}\right) + M_4 - 1\right] \quad (66)$$

where $M_5 = (\phi_T - \phi_R)r_1/(R - r_1)$. Therefore the TOA cdf for $t_T < t \le t_1$ can be expressed as

$$F^2_{t|E}(t \mid E) = 2(V_1 + V_2 + V_3 + V_4 + V_5)$$
$$\simeq \frac{k}{\pi\alpha(1+\xi)}(\alpha\xi\phi_R + 1 - \cos(\alpha\phi_R))$$
$$+ \frac{kM_2}{\pi}\left(\frac{\pi}{2} + \frac{tc}{L}\right)$$
$$+ \frac{kM_4}{\pi}\left[\frac{\pi}{2} - \phi_T - \frac{tc}{L} + \frac{\xi}{1+\xi}(\phi_T - \phi_R) + \frac{\cos(\alpha\phi_R) - \cos(\alpha\phi_T)}{\alpha(1+\xi)}\right]$$
$$+ \frac{2kM_3}{\sigma\sqrt{2\pi}}\left[Q\left(\frac{r_2}{\sigma}\right) - Q\left(\frac{r_1}{\sigma}\right)\right] + (f_\phi(\phi_R) + f_\phi(\phi_T))M_5\left[\frac{R\sqrt{2\pi}}{\sigma}Q\left(\frac{r_1}{\sigma}\right) + M_4 - 1\right]. \quad (67)$$

Therefore the complete expression of the TOA cdf becomes

$$F_{t|E}(t \mid E) = \begin{cases} F^1_{t|E}(t \mid E), & t_T < t \le t_{\max} \\ F^2_{t|E}(t \mid E), & t_{\min} < t \le t_T \\ 0, & \text{otherwise} \end{cases} \quad (68)$$

where $F^1_{t|E}(t \mid E)$ and $F^2_{t|E}(t \mid E)$ are defined by (56) and (67), respectively. The TOA pdf can be directly obtained by taking the derivative of (68) with respect to t. Denoting

$$r_1' = \frac{c(t^2c^2 + L^2 - 2Ltc\cos(\phi_T))}{2(tc - L\cos(\phi_T))^2}$$

$$\phi_R' = \frac{2c(tc - R)}{\sqrt{4R^2L^2 - (L^2 - t^2c^2 + 2tcR)^2}}$$

$$M_5' = \frac{Rc[t^2c^2 + L^2 - 2Ltc\cos(\phi_T)](\phi_T - \phi_R)}{2[R(tc - L\cos(\phi_T)) - r_2(tc + L)]^2} - \frac{r_2(tc + L)\phi_R'}{R[tc - L\cos(\phi_T)] - r_2(tc + L)}$$

$$M_6 = \frac{k}{2\pi(1+\xi)}[\alpha\phi_R'\cos(\alpha\phi_R)M_5 + (f_\phi(\phi_R) + f_\phi(\phi_T))M_5']$$

$$M_7 = \frac{k}{\pi}\left(\frac{\pi}{2} - \phi_T - \frac{tc}{L}\right) + (\phi_T - \phi_R) \times \left[\frac{k\xi}{\pi(1+\xi)} - f_\phi(\phi_R) - f_\phi(\phi_T)\right] + \frac{k(\cos(\alpha\phi_R) - \cos(\alpha\phi_T))}{\pi\alpha(1+\xi)}$$

the derivatives of $F^1_{t|E}(t \mid E)$ (56) and $F^2_{t|E}(t \mid E)$ (67) can be expressed as

$$f^1_{t|E}(t \mid E) \simeq \frac{kc}{\pi}(1-M_2)\left[\left(\frac{\pi}{2}+\frac{tc}{L}\right)\frac{r_2}{2\sigma^2}-\frac{1}{L}-\frac{M_3}{2\sigma^2}\right] + \frac{2ktc^2}{\sqrt{2\pi}\sigma L}Q\left(\frac{r_2}{\sigma}\right) \tag{69}$$

and

$$\begin{aligned} f^2_{t|E}(t \mid E) \simeq{}& \frac{2ktc^2}{\sqrt{2\pi}\sigma L}\left[Q\left(\frac{r_2}{\sigma}\right)-Q\left(\frac{r_1}{\sigma}\right)\right] \\ &+ \frac{\sqrt{2\pi}}{\sigma}RM_6Q\left(\frac{r_1}{\sigma}\right)+\frac{kcr_2}{2\pi\sigma^2}\left(\frac{\pi}{2}-1\right)(1-M_2) \\ &+ \frac{kc}{\pi L}(M_2-M_4) \\ &+ \left[\frac{kM_3r_1'}{\pi\sigma^2}+\frac{r_1r_1'M_7}{\sigma^2}-M_6+2\phi_R'f_\phi(\phi_R)\right](1-M_4) \end{aligned} \tag{70}$$

respectively.

REFERENCES

[1] Agarwal, N., Basch, J., Beckmann, P. Bharti, P., Bloebaum, S., Casadei, S. Chou, A. Enge, P., Fong, W., Hathi, N., Mann, W., Sahai, A., Stone, J., Tsitsiklis, J., and Roy, B. V.
Algorithms for GPS operation indoors and downtown.
GPS Solutions, **6**, 3 (Dec. 2002), 49–160.

[2] Steingass, A. and Lehner, A.
Measuring the navigation multipath channel—A statistical analysis.
ION GNSS 2004, Long Beach, CA, Sept. 21–24, 2004.

[3] Lehner, A. and Steingass, A.
A novel channel model for land mobile statellite navigation.
ION GNSS 2005, Long Beach, CA, Sept. 13–16, 2005.

[4] Braasch, M. S.
In B. Parksinon and J. Spilker (Eds.), *Multipath Effects, Global Positioning System: Theory and Applications*, vol. I.
Washington, D.C.: AIAA, 1996.

[5] Dierendonck, A. J., Fenton, P., and Ford, T.
Theory and performance of narrow correlator spacing in a GPS receiver.
NAVIGATION, Journal of the Institute of Navigation, **39**, 3 (Fall 1992), 265–283.

[6] Misra, P. and Enge, P.
Gobal Positioning System: Signals, Measurements, and Performance (2nd ed.).
Lincoln, MA: Ganga-Jamuna Press, 2006.

[7] Janaswamy, J.
Angle and time of arrival statistics for Gaussian scatter density model.
IEEE Transactions on Wireless Communications, **1** (July 2002), 488–497.

[8] Kong, S-H.
TOA and AOD statistics for down link Gaussian scatterer distribution model.
IEEE Transactions on Wireless Communications, **3** (May 2009), 2609–2617.

[9] Ertel, R. B. and Reed, J. H.
Angle and time of arrival statistics for circular and elliptical scattering models.
IEEE Journal on Selected Areas in Communications, **17** (Nov. 1999), 1829–1840.

[10] Papoulis, A.
Probability, Random Variables and Stochastic Processes (3rd ed.).
New York: McGraw-Hill, 1991.

[11] Braasch, M. S.
Autocorrelation sidelobe considerations in the characterization of multipath errors.
IEEE Transactions on Aerospace and Electronic Systems, **33** (Jan. 1997), 290–295.

[12] Goldsmith, A. J.
Wireless Communications.
London: Cambridge University Press, 2005.

Seung-Hyun Kong (M'08) received a B.S.E.E. from Sogang University, Korea, in 1992, an M.S.E.E. from Polytechnic University, New York, in 1994, and a Ph.D. degree in aeronautics and astronautics from Stanford University, Stanford, CA, in 2006.

From 1997 to 2000, he was a research member for CDMA standard development and mobile position location technology at Samsung Electronics, Inc., Korea. From 2000 to 2004, he worked for Nexpilot Inc., Korea, as an R&D lead for UMTS location system development. He was with Qualcomm, Inc., San Diego, CA, where he was engaged in developing advanced location technologies such as cooperative localization for mobile nodes and urban GPS enhancements from 2007 to 2009. In January 2010, he joined the Department of Aerospace Engineering, Korea Advanced Institute of Science and Technology (KAIST), Daejeon, Korea, where he is an Assistant Professor. His research interests include technologies for urban and indoor navigation, statistical analysis of urban multipath channels, and signal acquisition and detection algorithms.